Journal of Elementology ISSN 1644-2296

Khairia M. Al-Qahtani, Mohamed H.H. Ali, Afify G. Al-Afify 2020.
Synthesis and use of TiO_2@rGO nanocomposites in photocatalytic removal of chromium and lead ions from wastewater.
J. Elem., 25(1): 315-322. DOI: 10.5601/jelem.2019.24.2.1862

RECEIVED: 7 May 2019
ACCEPTED: 3 November 2019

ORIGINAL PAPER

SYNTHESIS AND USE OF TiO_2@rGO NANOCOMPOSITES IN PHOTOCATALYTIC REMOVAL OF CHROMIUM AND LEAD IONS FROM WASTEWATER

Khairia M. Al-Qahtani[1], Mohamed H.H. Ali[2], Afify G. Al-Afify[2]

[1] Department of Chemistry
Princess Nourah Bint Abdulrhaman University, Kingdom of Saudi Arabia
[2] Freshwater and Lakes Division
National Institute of Oceanography and Fisheries, Cairo, Egypt

Abstract

The photocatalytic removal of Cr(VI) and Pb(II) from different wastewater types using doped TiO_2 nanocomposites with reduced graphene oxide added in different ratios (1%, 3%, 5% w/w) and the removal of these ions from their aqueous solutions,were studied using batch adsorption methods. Different types of wastewater from agricultural, domestic and industrial sources were collected from several governorates in Egypt. Some physical characterization technologies, including X-ray diffraction (XRD), Fourier Transform infrared spectroscopy (FTIR) and scanning electron microscopy (SEM), were used to demonstrate the morphological characteristics of the surface of the synthesized sorbent. The surface area of TiO_2@rGO 1% was larger than that of TiO_2@rGO 3% or 5%. The nanocomposites showed high removal efficiency of toxic metals in different types of wastewater in the order of: Fe > Mn > Cd > Cr > Zn > Cu > Pb. In addition, some factors, e.g. pH, sorbent dosage, initial metal concentration and contact time, were studied. The results indicated that the maximum removal efficiency was achieved at pH = 2 and 5.5, 150 min contact time and 0.4 g L^{-1} sorbent dose for Cr(VI) and Pb(II), respectively. Langmuir and Freundlich isotherm studies showed that adsorption obeyed the Langmuir isotherm model. Metal ions were removed following the order of Cr(VI) > Pb(II) according to values of maximum adsorption capacities (q_{max}), Langmuir constant (b), separation factor (RL) and Freundlich intensity parameter (1/n).

Keywords: reduced graphene oxide, sorbent, nanoparticles, chromium, lead.

Mohamed H.H. Ali, PhD, National Institute of Oceanography and Fisheries (NIOF), Fresh Water and Lakes Division, 101 El Kasr Aini St., Cairo, Egypt, e-mail: mhha_ali@yahoo.com, telephone/fax, +2 02 42185320

INTRODUCTION

Contamination of water is regarded as one of the most dangerous environmental issues, as different hazardous pollutants including trace metals, organic matters, fertilizers, pesticides and industrial wastes are rapidly increasing in quantities, polluting the surface water resources (Schwarzenbach 2006). These hazardous substances cause high toxicity and pose a threat to aquatic fauna and flora, hence it is necessary to develop novel, efficient and environmental friendly techniques for water treatment (Luo et al. 2013, Martins et al. 2014).

Chromium and lead metals are non-biodegradable toxic pollutants. The rapid industrial progress, especially iron, steel and electroplating works as well as textile and dye manufacturing factories, are the most responsible for introducing these ions into the aquatic environment by discharging effluents directly to surface waters (Fang et al. 2007, Poursani et al. 2016). Contrarily, Cr(III) is almost nontoxic, and therefore converting Cr(VI) to Cr(III) by reduction is regraded as a key solution in the treatment of wastewater containing Cr(VI). A photo-reduction process using TiO_2 appears to be an effective way to reduce heavy metal ions in their aqueous solutions down to low toxicity states (Zhao et al. 2013). In recent decades, development of novel techniques for wastewater treatment has become an urgent necessity. Nano-compounds are extremely important in this regard, and have become a subject of comprehensive research conducted in order to design nanomaterials with specific characteristics concerning the size, shape and even surface properties. Such nanomaterials can give rise to the hope of solving multi-environmental problems through their beneficial applications (Gothandam et al. 2018). Due to their specific characteristics, especially high surface area and high ratio between the surface area and volume, these materials exhibit distinct properties, such as high potential catalytic efficiency and high reactivity. These features make them superior adsorbents in comparison with common compounds (Li et al. 2006, Hristovski et al. 2007).

Several studies have been carried out to overcome the limitation of TiO_2, and these efforts focused on diminishing the band gap of TiO_2 and on the inhibition of electron-hole recombination. These strategies used either doping TiO_2 with a metallic precursor (Kozlova, Vorontsov 2006) and a non-metallic one (Marschall, Wang 2014) or tested mixing TiO_2 with other nanoparticles (Almeida et al. 2016). Mixing TiO_2 with graphene (G) or graphene oxide (GO) at different doping ratios is among the most promising ways to synthesize TiO_2 nanocomposites (TiO_2@G and TiO_2@GO), and such nanocomposite materials have been improved in terms of both optical and electronic properties for photocatalytic processes (Martins et al. 2018). Nowadays, nanoparticles have become a good alternative to other traditional absorbents, able to obtain improved results in metal remediation from waters (Zhang 2003, Tratnyek, Johnson 2006, Vaseashta et al. 2007, Li et al. 2014).

This paper aims 1) to discuss the preparation and to determine characteristics of TiO_2@rGO nanocomposites, 2) to provide sufficient information about heavy metal adsorption from different types of wastewater by using TiO_2@rGO nanocomposites doped at different ratio as sorbents, 3) and to identify the factors that affect the photoreduction process by investigating the effects of pH, sorbent dose, and initial concentration of metal ions.

MATERIALS AND METHODS

All of the used chemicals were of analytical grade. They were used as received from Loba Chemie (India), while TiO_2 powder originated from Degussa Company (Germany).

Synthesis of TiO_2@rGO nanocomposites

Synthesis of rGO proceeded according to the modified Hummers' method (Hummers, Offeman 1958) using graphite powder (99.95%). The method was described in detail by Ali et al. (2018). Briefly, 5 g of graphite powder, 2.5 g of $NaNO_3$ and 60 ml concentrated H_2SO_4 were transferred to a 2 L flask in an ice bath, with the contents being stirred for 30 min. Then a dose of 15 g of $KMnO_4$ was added slowly, the temperature of the mixture was kept below 15°C for 12 h, after which a dose of 72 ml of distilled water was added carefully and the temperature of the mixture was raised to 50°C for another 12 h until the mixture's colour changed from yellowish-brown to bright yellow. Then, 22 ml H_2O_2 were added slowly, followed by continuous stirring for 3 h. TiO_2 nanoparticles were pretreated in a furnace at 500°C for 2 h, GO was added to absolute ethanol in a concentration of 0.5 mg ml^{-1}, the weight ratios of GO to TiO_2 of 1, 3 and 5 wt% were adjusted in the GO/ethanol solution, and the mixture was treated by ultrasounds for 30 min. Finally, the mixture was dried at 60°C for 12 h to obtain TiO_2@rGO nanocomposites.

Characterization

SEM and EDX were measured using a JEM-2100 (JEOL, Tokyo Japan) at an acceleration voltage of 200 kV. The XRD pattern was measured with a Philips X-Ray diffractometer Model PW-3710. The patterns were progressed with Ni-filtered copper radiation (λ = 1.5418°A; 30 kV and 10 mA) at a scanning rate of $2\theta = 5°$ min^{-1}. FTIR spectra were recorded using a spectrometer (6700FTIR, Nicolet, America). The samples were ground together with KBr (1:100) and placed in a sample holder. The measurements were recorded within the range of 4000-400 cm^{-1}. The surface area of nanocomposites was determined accoding to the BET (Brunauer–Emmett–Teller) method from nitrogen adsorption-desorption isotherms using a Coulter SA3100 instrument with outgas set at 150°C for 15 min (Brunauer et al. 1938).

Collection and photocatalytic treatment of wastewater samples

Wastewater samples represented different types of effluents: three samples from agricultural drains, three samples of domestic effluents and four samples of industrial waste (Table 1). Before the treatment, 500 ml of each sample was completely digested with 20 ml of concentrated nitric acid.

Each waste sample was treated with TiO_2@rGO nanocomposites doped at different ratios (1, 3 and 5% respectively) under the optimum condition for each absorbent (pH = 6, 0.4 g L^{-1} sorbent dose and 150 min duration time), after which the solution was centrifuged at 15 000 rpm for 15 min. The concentrations of Fe, Mn, Cu, Zn, Cr, Pb, and Cd were measured in both the digested and treated samples using ICP-AES (Inductively Coupled Plasma-Atomic Emission Spectroscopy; Spectro Genesis, Germany).

Table 1

Different collected samples of wastewater

Samples No.	Name of drain	Type of waste
1	El-Wadi	agricultural drain
2	El-Bats	
3	El-Serw	
4	El-Qalaa	domestic drain
5	El-Rahawy	
6	Bahr El-Baqr	
7	textile factory	industrial wastes
8	sugar factory	
9	petrochemical factory	
10	iron and steel factory	

Batch adsorption study

Serial standard solutions of Cr(VI) and Pb(II) were prepared from stock solution (1000 mg L^{-1}) of each metal using analaR® grade of $K_2Cr_2O_7$ and $Pb(NO_3)_2$ salts dissolved in deionized water; the pH of each solution was adjusted to the desired degree using diluted HNO_3 or NaOH solution. Photocatalytic adsorption of Cr(VI) and Pb(II) was studied using a 300W mercury lamp with a cut-off filter (λ > 400 nm) as a light source. The effects of pH changes, duration of the irradiation time, a photocatalyst's dose and initial metal concentrations were studied with respect to the photocatalytic process factors. To establish the adsorption-desorption equilibrium, the solutions were stirred in the dark for 30 min, then the samples were centrifuged for 10 min at 15 000 rpm. Cr and Pb concentrations were measured using ICP-AES (Inductively Coupled Plasma-Atomic Emission Spectroscopy;

Spectro Genesis, Germany). The adsorption capacity of heavy metal ions by a different microbial mat could be expressed as follows (Horsfall et al. 2006, Zulkali et al. 2006):

$$q_e = \frac{(C_0 - C_e) \cdot V}{M},$$

$$R\% = \frac{(C_0 - C_e) \cdot 100}{C_0},$$

Where: C_0 – initial metal ion concentration, C_e – concentration of metal ions in a solution (mg L^{-1}) at equilibrium, C_t – concentration of metal ions in a solution (mg L^{-1}) at time t in solution, V – volume of initial metal ions in the solution used (L) and M – mass of the adsorbent used (g).

RESULTS AND DISCUSSION

Characteristics

SEM analyses were applied to the synthesized nanocomposites in order to describe their morphological shapes. Figure 1*a-c* shows SEM images at different magnification, revealing irregular shapes, which correspond to an irregular structure of nanocomposites, and with many surface pores, cracks and the evident roughness of particles, all leading to a greater surface area. The elemental composition of the three synthesized nanocomposites (TiO_2@ rGO 1%, 3% and 5%) was determined by EDX spectra, which showed that within the energy range of 0 - 5 keV the dominant elements were Ti, C, O, K, N (Figure 1*a-c*). The appearance of a gradually increasing carbon content (13.32, 15.29 and 17.53%) at different nanocompositedoping ratios, respectively, indicates that TiO2@rGO has been successfully synthesized (Gohel et al. 2017). The crystalline structure of the prepared TiO_2@rGO particles was demonstrated based on the XRD spectrum pattern (Figure 2). All observed diffraction peaks were matched to the characteristics of the TiO_2 crystal plane for both: anatase A (25.28°, 37.8°, 48.03°, 54.04°, 55.5°, and 69.9° peaks) which corresponds to (101), (004), (200), (105), (211) and (204) crystal planes, and rutile phase R (27.39° and 36.11°) which corresponds to the (110) and (101) of crystal phases (JCPDS Card No.21-1272 and 21-1276, respectively) (Martins et al. 2018). A remarkable disappearance of the GO peak at the expected moment (23°-24°) may be due to their low concentrations in the composites or the peak may have been overshadowed or overlapped by a strong (101) peak of the TiO_2 anatase phase at 25.28°, which is in good agreement with the results obtained by Blanton, Majumdar (2013).

The FTIR spectra (Figure 3) for 1%, 3% and 5 % of TiO_2@rGO nanoparticles show various strong absorption peaks; stretching vibration water

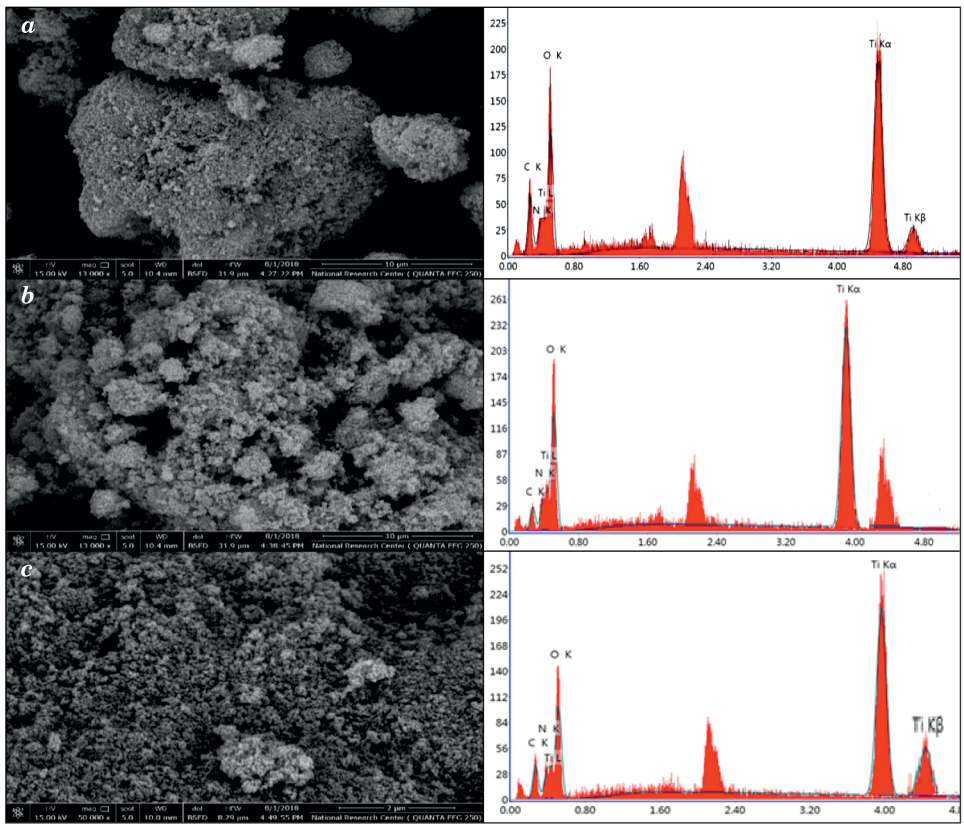

Fig. 1. Scanning electron microscope (SEM) and related X-Ray spectra (EDX) for: *a* – 1% TiO_2@rGO, *b* – 3% TiO_2@rGO and *c* – 5% TiO_2@rGO nanocomposites

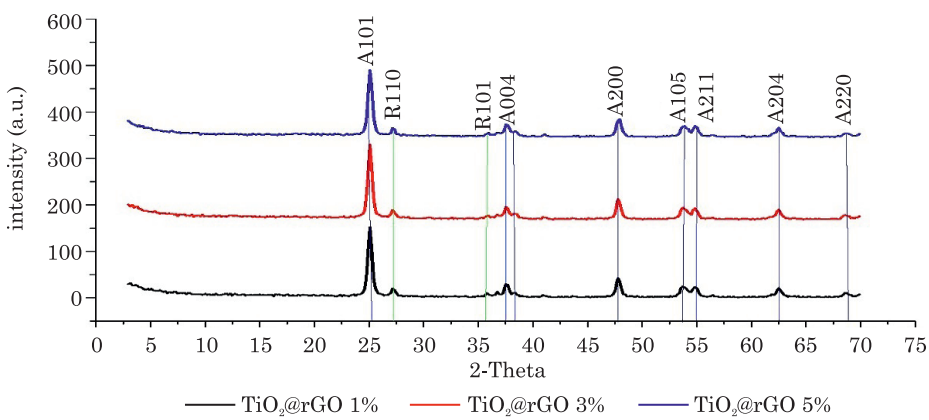

Fig 2. XRD Spectrum models of TiO_2@rGO nanoparticles: A – anatase phase planes, R – rutile phase planes

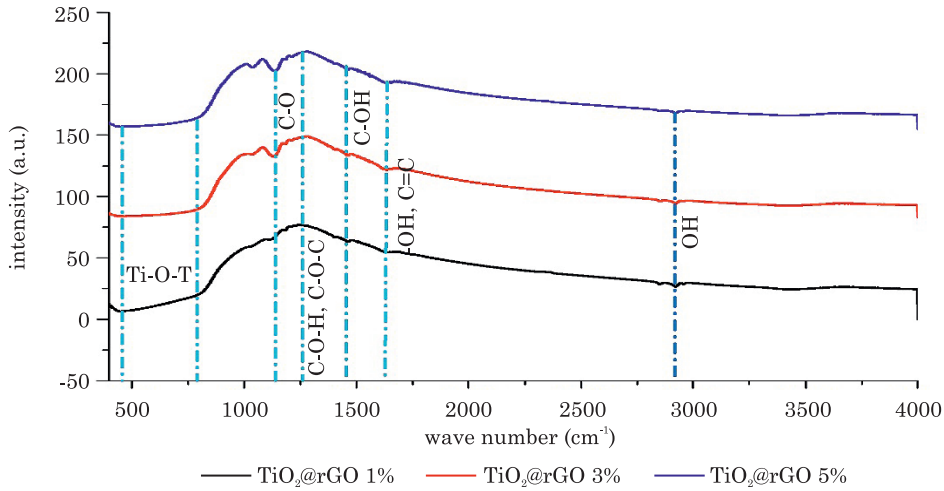

Fig. 3. Spectra of FTIR of 1% TiO2@GO, 3% TiO2@rGO and 5% TiO_2@rGO nanocomposites

–OH around 2900 cm^{-1}, while vibration band at 1630 cm^{-1} corresponds to bending –OH and stretching C=C; it is also possible to identify the peaks corresponding to hydroxyl C-OH (1410 cm^{-1}) and epoxy C-O (1250 cm^{-1}) (Wang et al. 2012). In addition, a remarkable wide peak was observed between 450-900 cm^{-1}, indicating stretching vibration of Ti–O–Ti bonds, which indicates that pure TiO_2 is found higher than 90% (Martins et al. 2018).

Specific surface area (S_{BET}) of the prepared nanocomposites (1%, 3% and 5%) was determined using the isotherms of N_2 sorption-desorption (Table 2,

Table 2

The specific surface area, radius and pore volume obtained TiO_2@rGO composites

Samples	S_{BET} (m^2 g^{-1})	r (nm)	V_{Ptotal} (cm^3g^{-1})
1% TiO_2@rGO	78.185	9.094	0.0885
3% TiO_2@rGO	58.055	12.630	0.0971
5% TiO_2@rGO	62.22	10.17	0.0833

Figure 4). The three composites show mesopores with a hole in the range of 9.1-12.63 nm (Table, 2). TiO_2@rGO 1% had the highest value of surface area of about 78 m^2 g^{-1}, followed by 5% TiO_2@rGO with S_{BET} about 62.22 m^2 g^{-1}, while 3% TiO_2@rGO composites came last with their S_{BET} of 58 m^2 g^{-1}.

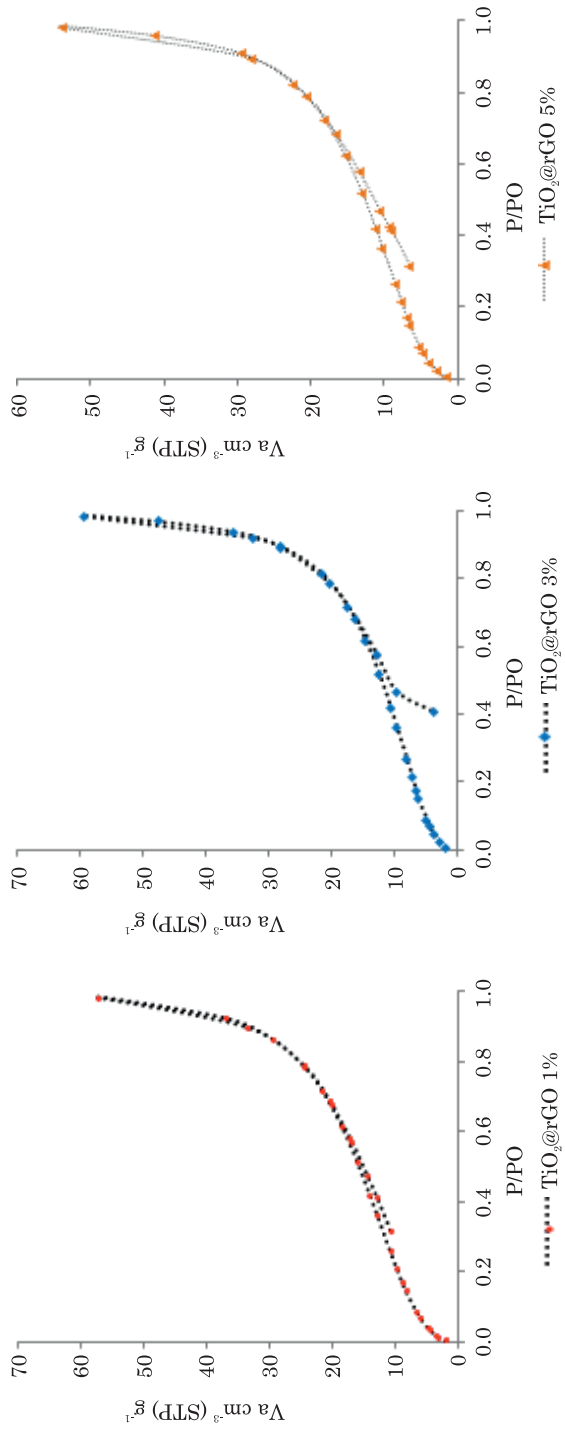

Fig. 4. N_2 sorption-desorption isotherms of prepared nanocomposites

Batch biosorption experiments

Effect of pH

The adsorption of inorganic pollutants, e.g. heavy metal, from an aqueous solution is largely depend on the pH of the solution, which is considered to be a major factor affecting protonation of functional groups on the surface of a sorbent (Hu et al. 2006). Figure 5 illustrates the adsorption ratio of Cr(IV) and Pb(II) at different pH values within the range of 2 to 5.5 under specific conditions (50 mg L^{-1} initial metal concentration, 0.4 g L^{-1} dose of a nanocomposite and 180 min duration time).

The results showed a higher removal rate owing to a gradual increase in pH, reaching the maximum values of 91% and 89.2% at pH = 2 and 6 for Cr(IV) and Pb(II), respectively (Figure 5*a*,*b*). As it is known, the presence

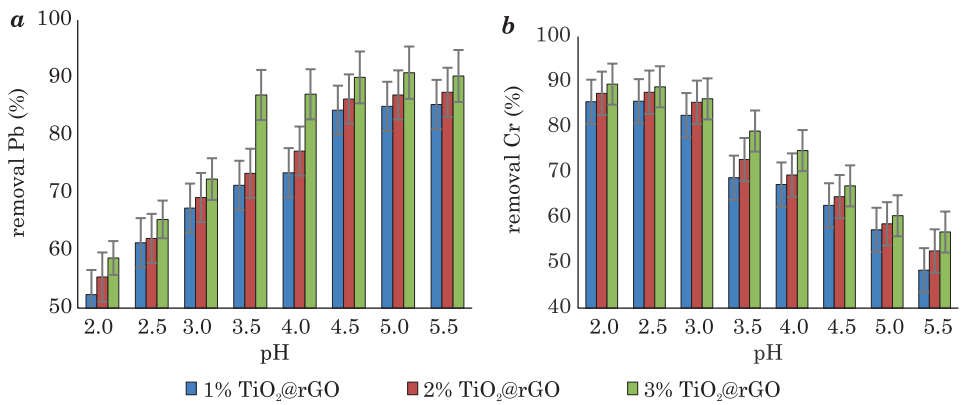

Fig. 5. Effect of pH on the adsorption of: a – Pb(II) and b – Cr(VI).

Effect of irradiation time

of Cr(IV) ions depends on the pH of a solution. Hydrogen chromate ($HCrO_4^-$) is present as a major form of the element at 1 < pH < 7, but when pH is above 7 dichromate ($Cr_2O_7^{-2}$) becomes the dominant form (Jabeen et al. 2011). Our results indicate that TiO_2@rGO nanocomposites adsorbed Cr(VI) optimally at pH = 2, when the removal percentage peaked at 89.2%, hence the prevalent form chromium under these conditions was hydrogen chromate ($HCrO_4^-$). Our data coincidence with findings by Joshi, Shrivastava (2011), who reported that the highest removal of Cr(VI) (96.8%) was achieved at pH = 2, while decreasing to 85% at pH = 3. Moreover, Fu et al. (2019) confirmed optimum pH values to be equal 5 for the highest Cd(II) removal, when it could reach 100% removal efficiency on the surface of a titanate/TiO_2 sorbent. Also, Li et al. (2014) indicated that maximum sorption of Cr (VI) on the surface of Fe_3O_4@mTiO_2@GO was achieved at pH 2 (Table, 3). Furthermore, the results showed that TiO_2@rGO 5% could ensure the highest removal percentage, between 91 and 89.2%, at pH = 5.5 and 2 for Pb and Cr ions, respectively, while the lowest removal percentage (52 and 48%) was achieved using TiO_2@rGO 1% as a sorbent (Figure 5).

Table 3

List of various sorbents and their removal efficiencies of different heavy metals

Used sorbent	Studied heavy metals	pH	Kinetics	Time (min)	Efficiency (%)	Reference
TiO_2-RGO	Cr (VI)	2	*	200	86	Zhao et al. (2013)
Fe_3O_4@mTiO_2@GO	Cr (VI)	2	pseudo 2nd order	40	~ 90	Li et al. (2014)
Chitosan/TiO_2	Cu(II), Pb(II)	6	pseudo 1st order	30	95	Razzaz et al. (2016)
Nano-TiO2	Pb (II)	6	pseudo 1st order	240	85	Poursani et al. (2016)
TiO_2/ZnO	V(V), Pb (II)	6.1	pseudo 2nd order	30	> 90	Yin et al. (2018)
Titanate/TiO_2	Cu(II), Cd(II)	6	*	15	92	Fu et al. (2019)
TiO_2@rGO	Cr(VI), Pb (II)	2, 5.5	pseudo 2nd order	150	89 - 93	current data

Effects of irridiation time ranging from 15 to 180 min on the adsorption of Cr(VI) and Pb(II) on the surface of 0.4 g L^{-1} TiO_2@rGO nanoparticles using 50 mg L^{-1} initial metal concentration are illustrated in Figure 6. Remarkably, the removal efficiency for both metal ions increased with the longer irradiation time until reaching the equilibrium stage, which was due to active binding sites being abundant on the surface of the sorbent, but the adsorption process gradually decreased with the passage of time as a result of gradual occupancy of active sites (Ali et al. 2019). High removal percentage equal 88% and 89% was observed for Pb(II) and Cr(VI), respectively, after 150 min and the rate of removal was steady. Zhao et al. (2013) showed that the maximum duration time to achieve maximum adsorption of Cr(VI) at 86% efficiency rate on the surface of TiO2@rGO was 200 min (Table 3).

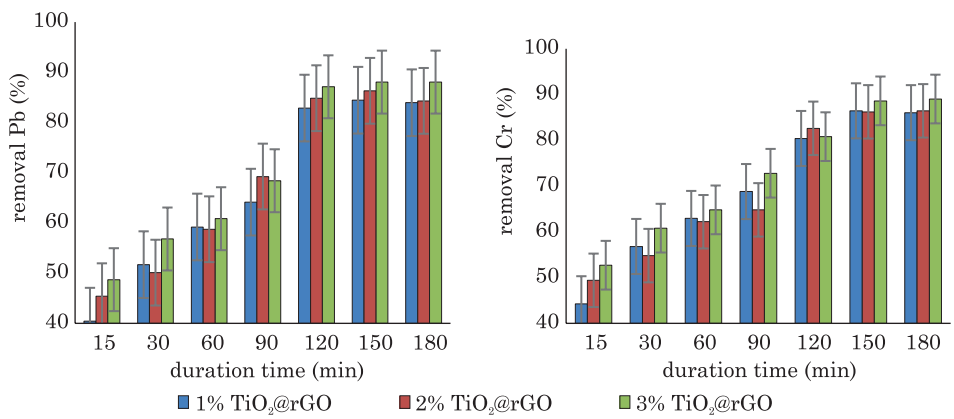

Fig. 6. Effect of contact time on the adsorption of: *a* – Pb(II) and *b* – Cr(VI)

Effect of a dose of sorbent

A sorbent's dose has a great impact on adsorption (Moghadam et al. 2013). Different doses (0.1 - 1 g L^{-1}) of the three prepared nanocomposites were used to assess the efficiency of the removal of metals ions (Figure 7).

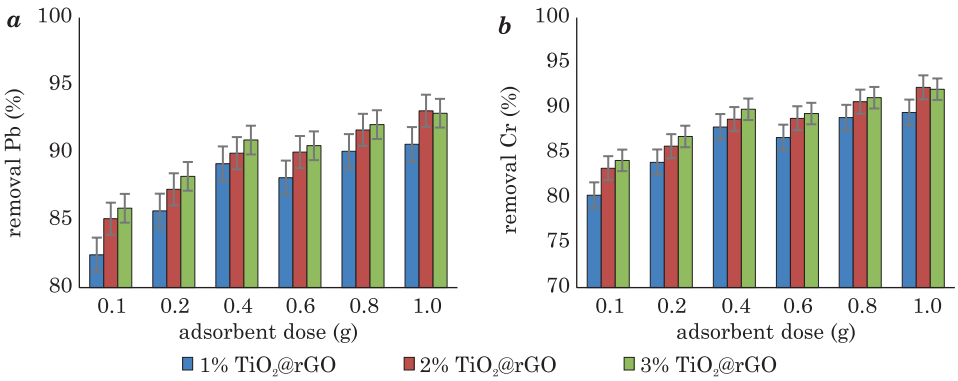

Fig. 7. Effect of a sorbent's dose on the adsorption of: *a* – Pb(II) and *b* – Cr(VI)

The results revealed slight variation in the removal efficiency between the three used nanocomposites although TiO_2@rGO 5% achieved the highest removal percentage. Moreover, our results showed greater removal capacity when the dose of a sorbent was higher, which was a consequence of the greater abundance of the superficial active binding sites on any of the different sorbents used. TiO_2@rGO 5% nanoparticles maintained the maximum removal percentage of 91 and 90% for Pb (II) and Cr (VI), respectively. On the other hand, all the highest removal values were achieved at 0.4 g L^{-1} for the three used sorbents.

Effect of initial concentrations of metals

Different series of initial metal concentrations (5, 10, 15, 20, 25 and 50 mg L^{-1}) were tested to determine the removal efficiency at a dose of nanoparticles of 0.4 g L^{-1}, and the duration time of 150 min (Figure 8). The results showed a gradual increase in the removale percentage of metals, reaching 93% for both Pb(II) and Cr(VI), when the initial concentrations of the metals were raised (to 50 mg L^{-1}), which was due to the metals that tended to be adsorbed to active binding sites on the sorbent's surface. However, further increase in the concentrations of the metals lead to the occupation of binding sites until saturation and then equilibrium were attained (Sudarsan et al. 2015).

Photocatalytic removal of heavy metals from wastewater

Distribution of heavy metals in different drains

The distribution of heavy metals in wastewater from different types of drains is shown in Table 4. Fe values followed by Mn were the highest

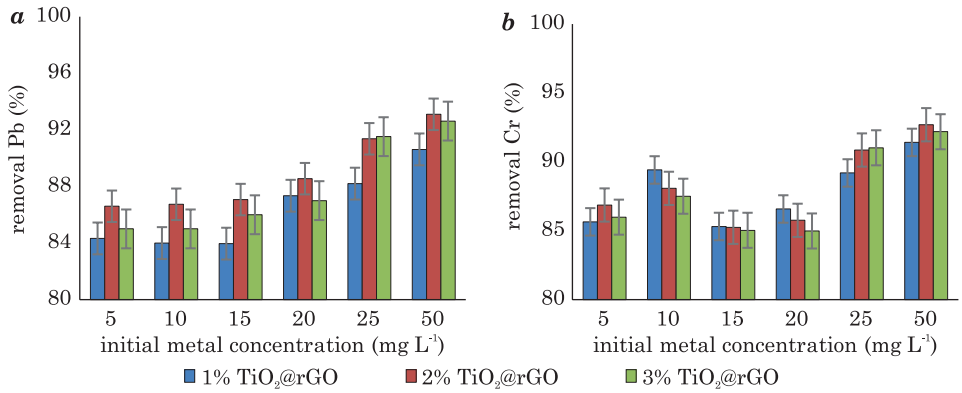

Fig. 8. Effect of initial concentrations of the metals on the adsorption of: *a* – Pb(II) and *b* – Cr(VI)

Table 4

Concentrations of some heavy metals (μg L^{-1}) in different types of wastewater

Name of the drain	Fe	Mn	Cu	Zn	Cr	Pb	Cd
El-Wadi	389	157	21	36	15	14	3
El-Bats	450	215	29	34	27	18	5
El-Serw	350	152	35	45	26	29	15
El-Qalaa	951	248	115	65	48	105	36
El-Rahawy	1105	365	101	89	59	39	14
Bahr El-Baqr	875	415	87	68	47	28	19
Textile factory	3152	987	265	178	325	247	105
Sugar factory	289	147	26	48	25	15	12
Petrochemical factory	857	354	75	115	45	29	16
Iron and steel factory	826	314	36	57	90	36	28

among all the measured metals, while Cd concentrations achieved the lowest values. On the other hand, industrial wastewater, especially from a textile factory, had the highest concentrations of all the measured metals; it was followed in this respect by samples of wastewater from Bahr El-Baqr Drain (domestic effluents). Agricultural wastewater had the lowest heavy metal content. These data were in good agreement with results obtained by Ali (2008), Ali et al. (2017) and Abdel-Satar et al. (2017) in their studies of heavy metal distribution.

Removal of heavy metals from different types of wastewater

The three different nanocomposites were applied to different wastewater samples for studying their capabilities to remove seven toxic heavy metals (Figure 9), and the results indicated that TiO_2@rGO with different GO

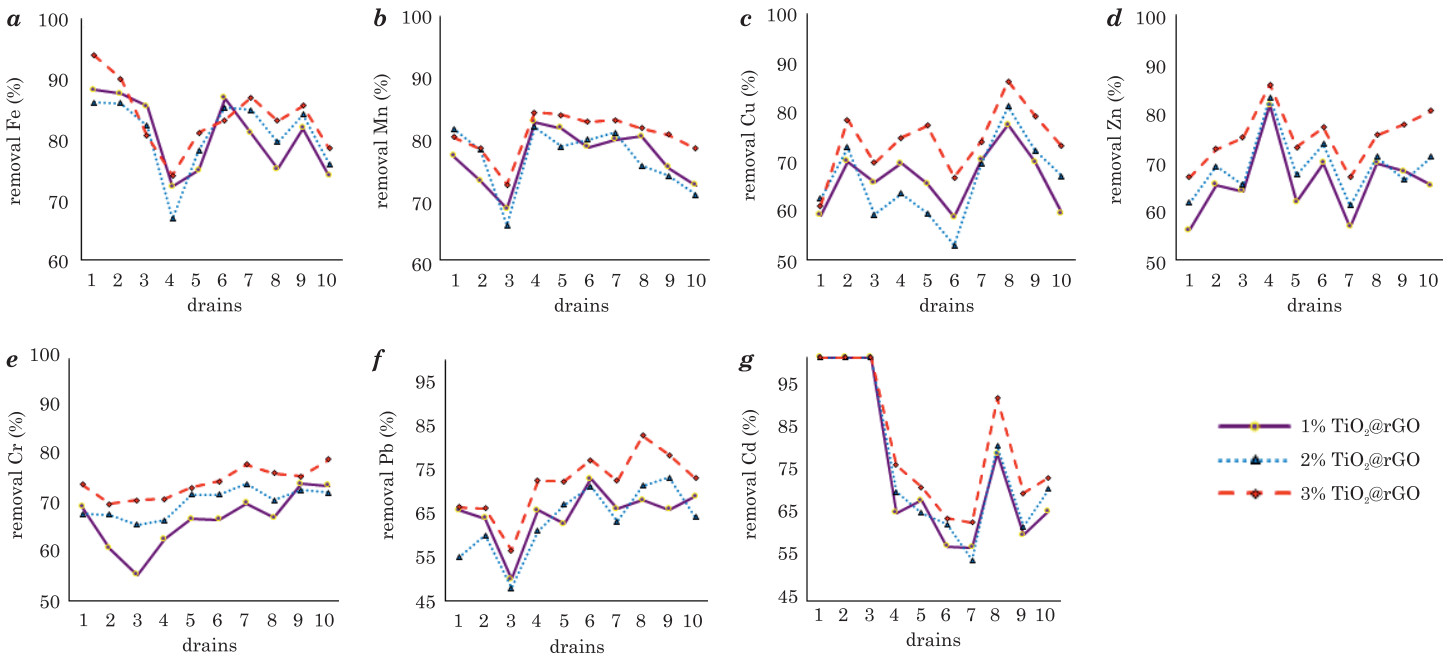

Fig. 9. Removal percentage of different heavy metals in different types of wastewater using TiO_2@rGO sorbents

doping ratios is a promising sorbent for all the studied metals. Figure 9 clearly shows that TiO_2@rGO 5% achieves the highest removal rate ranged between 57 - 100% in comparison with 1% and 3% doped nanocomposites, which showed negligible differences in removal efficiency for all the metals. Moreover, the removal efficiency increased at low concentrations of Fe and Cd, which is the same observation as made by GOHEL et al. (2017) for cadmium removed with the application of ZnO-GO nanocomposites. Furthermore, the adsorption capacities were improved at considerably elevated values of Mn, Cr, Cu, Zn and Pb.

The adsorption results revealed that Fe reached the highest removal percentage in comparison with the other metals, ranging between 67% to 94%, followed by Mn with the range of 66% - 84%, while Pb had the lowest removal percentage of 47% at a low Pb ion concentration in wastewater fron the agricultural drain (Figure 9). Generally, removal efficiency of the toxic metals by the three nanocomposites was in the order of Fe > Mn > Cd > > Cr > Zn > Cu > Pb.

Adsorption isotherms

Two isotherm models (Langmuir and Freundlich) were used to describe the adsorption process by analyzing the isotherms. The Langmuir model suggests homogeneity of the surface of an adsorbent, while the Freundlich isotherm assumes the diversity of adsorption sites. Both Langmuir and Freundlich constants and isotherm graphs are shown in Table 4 and Figures 9 and 10.

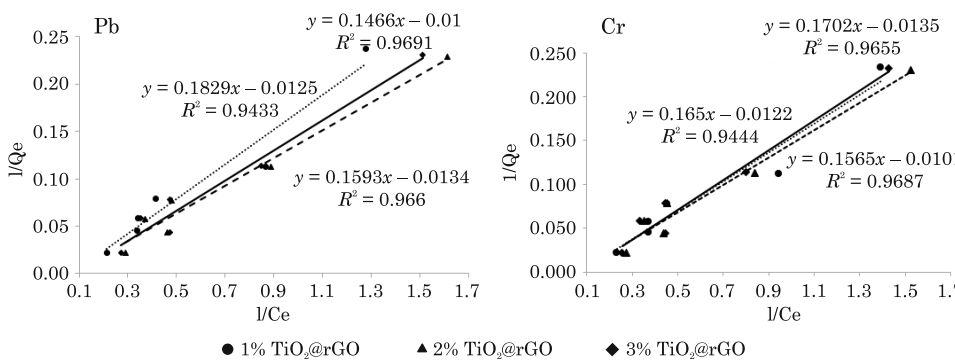

Fig. 10. Langmuir isotherm plot for adsorption of Pb(II) and Cr(VI) ions by TiO_2@rGO sorbents

The Langmuir model is expressed by the equation:

$$q_e = \frac{q_{\max} b C_e}{1 + b C_e},$$

$$1/q_e = 1/q_{\max} + (1)/(bq_{\max})(1)/C_e,$$

where: q_{max} (mg g^{-1}) – maximum uptake of sorbate, b (L mg^{-1}) – Langmuir constant, q_e (mg g^{-1}) – amount of metal adsorbed; and C_e (g L^{-1}) – metal concentration at equilibrium

The Freundlich isotherm model is described by the following equation:

$$q_e = K_f C_e^{1/n},$$

$$\log q_e = \log K_f + 1/n \log C_e,$$

where: q_e – amount of metal adsorbed by biosorbent (mg g^{-1}), C_e – equilibrium adsorbate concentration (mg L^{-1}), K_f – adsorbent capacity, n – adsorption intensity determined from the linear plot

The equilibrium data of different TiO_2@rGO used for removal os Cr(VI) and Pb(II) were fitted the best with the Langmuir model at $R^2 > 0.94$, while the corresponding R^2 for the Freundlich model < 0.90 (Table 5, Figures 10, 11).

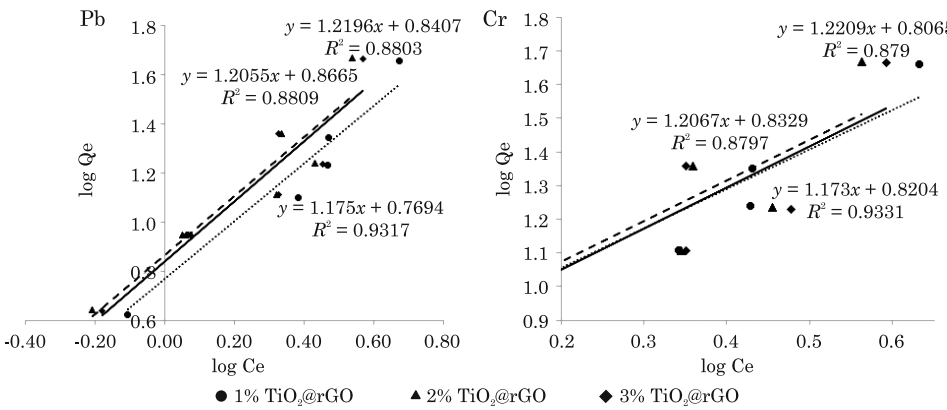

Fig. 11. Freundlich isotherm plot for adsorption of Pb(II) and Cr(VI) ions by TiO_2@rGO sorbents

Therefore, the monolayer adsorption of metal ions onto the homogenous surface of adsorbents is the favorite suggestion. According to b values, the used sorbents had high affinity with the metals in the order Cr(VI) > Pb(II). The separation factor or dimensionless constant (R_L) which predict the affinity between the sorbate and sorbent could be used as essential features of the Langmuir adsorption isotherm. R_L factor is expressed as:

$$R_L = \frac{1}{1 + bC_i},$$

where: C_i – initial concentration and b – Langmuir constant. R_L values determine the Langmuir isotherm type: if (R_L = 0) irreversible, (R_L = 1), linear, (R_L > 1), unfavorable or (0 < R_L < 1) mean favorable adsorption (McKay et al. 1982). The R_L values obtained in the present study ranged from 0.19 to 0.24 (Table 5), indicating favorable adsorption of the studied metal ions onto all used sorbents. On the other hand, the intensity parameter of Freundlich

Table 5

Constants of the Langmuir and Freundlich isotherms for Pb and Cr adsorption by different nanoparticle sorbents

Metal	Langmuir												Freundlich								
	1% TiO_2@rGO				3% TiO_2@rGO				5% TiO@rGO				1% TiO2@rGO			3% TiO_2@rGO			5% TiO_2@rGO		
	b	q_{max}	R_L	R^2	b	q_{max}	R_L	R^2	b	q_{max}	R_L	R^2	K_f	n	R^2	K_f	n	R^2	K_f	n	R^2
Pb	0.07	80	0.23	0.94	0.08	75	0.19	0.97	0.07	100	0.23	0.97	5.88	0.85	0.93	7.35	0.83	0.88	6.93	0.82	0.88
Cr	0.08	82	0.21	0.94	0.09	99	0.24	0.97	0.08	74	0.20	0.97	6.61	0.85	0.93	6.81	0.83	0.87	6.40	0.82	0.88

(1/n) is a function of the adsorption strength in the adsorption process (Voudrias et al. 2002), since n value illustrates the degree of nonlinearity between adsorption and the concentration of solution; in the case of n = 1 adsorption is linear, at n < 1 adsorption is a chemical process, and adsorption is a physical process if n > 1 (Desta 2013). The current data showed that n values were almost < 1 (Table 5), which confirms good chemical absorption of the studied metals onto the surface of the three used sorbents.

CONCLUSION

Synthesizing and using of TiO_2@rGO nanocomposites as sorbents proved to be a promising solution, showing enhanced performance in the removal of toxic metals from different types of wastewater. Therefore, removal of heavy metals from industrial, domestic or agricultural wastewater can be achieved by using nanocomposite sorbents. Cr ions were bound with TiO_2@rGO and mostly reduced to the trivalent form. The maximum adsorption and photocatalytic reduction of Cr(VI) and Pb(II) was achieved at pH = 2 and 5.5, 0.4 g L^{-1} sorbent doses, 150 min contact time and 50 ppm initial metal concentration, respectively.

ACKNOWLEDGEMENTS

This research was supported by the Chair of Environmental Pollution Research at Princess Nourah bint Abdulrahman University (Grant no. EP-03).

REFERENCES

Abdel-Satar A.M., Ali M.H., Goher, M.E. 2017. *Indices of water quality and metal pollution of the Nile River, Egypt*. Egypt J Aquat Res, 43(1): 21-29.

Ali M.H. 2008. *Assessment of some water quality characteristics and determination of some heavy metals in Lake Manzalah, Egypt*. J. Aquat. Biol. Fish., 12(2): 133-154.

Ali M.H., Abd Elkarim M.S., Haroun S.A., Attwa K.M. 2019. *Bioremediation of Fe, Zn and Cd ions from aqueous solution using dead cells of cyanobacterial mats from extreme habitat, Siwa Oasis, Egypt*. Egypt. J. Aquat. Biol. Fish., 22(5): 511-522.

Ali M.H., Abdel-Satar A.M., Goher, M.E. 2017. *Present status and long-term changes of water quality characteristics in heavily polluted Mediterranean Lagoon, Lake Mariut, Egypt*. IJRDO-J Appl Sci, 3(4): 1-18.

Ali M.H., Al-Afify D., Goher, M.E. 2018. *Preparation and characterization of graphene – TiO_2 nanocomposite for enhanced photodegradation of Rhodamine-B dye*. Egypt J Aquat Res, 44(4): 263-270.

Almeida N., Martins P., Teixeira S., Lopes da Silva J., Sencadas V., Kühn K. 2016. *TiO_2/ /graphene oxide immobilized in P(VDF-TrFE) electrospun membranes with enhanced visible-light induced photocatalytic performance*. J Mater Sci., 51: 6974-6986.

Blanton T., Majumdar D. 2013. *Characterization of x-ray irradiated graphene oxide coatings using x-ray diffraction, x-ray photoelectron spectroscopy, and atomic force microscopy*. JCPDS Int Cent Differ Data, 116-122.

Brunauer S., Emmett P.H., Teller E. 1938. *Adsorption of gases in multimolecular layers*. J Am Chem Soc., 60: 309-319.

Desta M.B. 2013. *Batch sorption experiments: Langmuir and Freundlich isotherm studies for the adsorption of textile metal ions onto teff straw (Eragrostis tef) agricultural waste*. J Thermodyn, ID: 375830, 6 pages.

Fang J., Gu Z.M., Gang D.C., Liu C.X., Ilton E.S, Deng B.L. 2007. *Cr(VI) removal from aqueous solution by activated carbon coated with quaternized poly(4-vinylpyridine)*. Environ. Sci. Technol., 41 : 4748.

Fu Y., Liu X., Chen G. 2019. *Adsorption of heavy metal sewage on nano-materials such as titanate/TiO_2 added lignin*. Results in Physics, 12: 405-411.

Gohel V.D., Rajput A., Gahlot S., Kulshrestha V. 2017. *Removal of toxic metal ions from potable water by graphene oxide composites*. Macromolecular Symposia, 376(1): p. 1700050 (1-4).

Gothandam K.M., Ranjan S., Dasgupta N., Ramalingam C., Lichtfouse E. 2018. *Nanotechnology,* food security and water treatment. (Vol. 11). Springer.

Horsfall M.J., Abia A.A., Spiff A. I. 2006. *Kinetic studies on the adsorption of Cd^{2+}, Cu^{2+} and Zn^{2+} ions from aqueous solutions by cassava (Manihot esculenta) tuber bark waste*. J. Biores. Technol., 97(35): 283-291.

Hristovski K., Baumgardner A., Westerhoff P. 2007. *Selecting metal oxide nanomaterials for arsenic removal in fixed bed columns: from nano-powders to aggregated nanoparticle media*. J. Hazard. Mater., 147(1): 265-274.

Hu J., Chen G., Lo I.M. 2006. *Selective removal of heavy metals from industrial wastewater using maghemite nanoparticle: performance and mechanisms*. J Environ Eng, 132(7): 709-715.

Hummers W.S., Offeman R.E. 1958. *Preparation of graphitic oxide*. J Am Chem Soc., 80: 1339-1339.

Jabeen H., Chandra V., Jung S., Lee J.W., Kim K.S., Kim K.M/.2011. *Enhanced Cr(VI) removal using iron nanoparticle decorated graphene*. Nanoscale, 3: 3583-3585.

Joshi K.M., Shrivastava V.S. 2011. *Photocatalytic degradation of chromium (VI) from wastewater using nanomaterials like TiO_2, ZnO, and CdS*. Appl. Nanosci, 1(3): 147-155.

Kozlova E.A., Vorontsov A.V. 2006. *Noble metal and sulfuric acid modified TiO_2 photocatalysts: mineralization of organophosphorous compounds*. Appl Catal B Environ., 63: 114-123. http://dx.doi.org/10.1016/j.apcatb.2005.09.020

Li L., Fan M., Brown R.C., Van Leeuwen J., Wang J., Wang W., Zhang P., 2006. *Synthesis, properties, and environmental applications of nanoscale iron-based materials: a review*. Crit. Rev. Environ. Sci. Technol., 36(5): 405-431.

Li Z., Feng X., Bi X., Li G., Lin Y., Sun G. 2014. *Probing the distribution and contamination levels of 10 trace metal/metalloids in soils near a Pb/Zn smelter in Middle China*. Environ. Sci. Pollut. Control Ser., 21(6): 4149-4162.

Luo Y., Guo W., Ngo H.H., Nghiem L.D., Hai F.I., Zhang J., et al. 2014. *A review on the occurrence of micropollutants in the aquatic environment and their fate and removal during wastewater treatment*. Sci Total Environ., 473-474: 619-641.

Marschall R., Wang L. 2014. *Non-metal doping of transition metal oxides for visible-light photocatalysis*. Catal Today, 225:111-135. http://dx.doi.org/10.1016/j.cattod. 2013.10.088

Martins P.M., Ferreira C.G., Silva A.R., Magalhães B., Alves M.M., Pereira L., Lanceros-Méndez S. 2018. *TiO_2/graphene and TiO2/graphene oxide nanocomposites for photocatalytic applications: A computer modeling and experimental study*. Composites (Part B): Engineering, 145: 39-46.

Martins P.M., Gomez V., Lopes A.C., Tavares C.J., Botelho G., Irusta S. 2014. *Improving photocatalytic performance and recyclability by development of Er-doped and Er/Pr-codoped TiO_2/poly(vinylidene difluoride)–trifluoroethylene composite membranes*. J Phys Chem C., 118: 27944-27953. http://dx.doi.org/10.1021/jp509294v.

McKay G., Blair H.S., Gardner J.R. 1982. *Adsorption of dyes on chitin*. J Appl Polymer Sci, 27(8): 3043-3057.

Moghadam M.R., Nasirizadeh N., Dashti Z., Babanezhad E. 2013. *Removal of Fe (II) from aqueous solution using pomegranate peel carbon: equilibrium and kinetic studies*. Int J Ind Chem, 4(1): 19-29.

Poursani A. S., Nilchi A., Hassani A., Shariat S. M., Nouri J. 2016. *The synthesis of nano TiO_2 and its use for removal of lead ions from aqueous solution*. J Water Res Protect, 8(04): 438.

Poursani A., Nilchi A., Hassani A., Shariat S., Nouri J. 2016. *The synthesis of nano TiO_2 and its use for removal of lead ions from aqueous solution*. J Water Res Protect, 8: 438-448. DOI: 10.4236/jwarp.2016.84037

Razzaz A., Ghorban S., Hosayni L., Irani M., Aliabadi M. 2016. *Chitosan nanofibers functionalized by TiO2 nanoparticles for the removal of heavy metal ions*. J Taiwan Inst Chem Engin, 58: 333-343.

Schwarzenbach R. 2006. *The challenge of micropollutants in aquatic systems*. Sci Technol., 313: 1072-1077. http://dx.doi.org/10.1126/science.1127291

Sudarsan J.S., Prasanna K., Baskar G., George R.B. 2015. *Role of titanium oxide nanoparticle in heavy metal reduction in electroplating waste water treatment*. Int J Chem Tech Res, 7(2): 547-553.

Tratnyek P.G., Johnson R.L. 2006. *Nanotechnologies for environmental cleanup*. Nano Today, 1(2): 44-48.

Vaseashta A., Vaclavikova M., Vaseashta S., Gallios G., Roy P., Pummakarnchana O. 2007. *Nanostructures in environmental pollution detection, monitoring, and remediation*. Sci Technol Adv Mat, 8(1-2): 47.

Voudrias E., Fytianos K., Bozani E. 2002. *Sorption–desorption isotherms of dyes from aqueous solutions and wastewaters with different sorbent materials*. Global Nest Int J., 4(1): 75-83.

Wang P., Wang J., Wang X., Yu H., Yu J., Lei M. 2012. *One-step synthesis of easy recycling TiO_2-rGO nanocomposite photocatalysts with enhanced photocatalytic activity*. Appl Catal B., 132-133: 452-459. http://dx.doi.org/10.1016/j.apcatb..12.009

Yin X., Meng X., Zhang Y., Zhang W., Sun H., Lessl J. T., Wang N. 2018. *Removal of V (V) and Pb (II) by nanosized TiO_2 and ZnO from aqueous solution*. Ecotoxicol Environ Safety, 164: 510-519.

Zhang W.X. 2003. *Nanoscale iron particles for environmental remediation: an overview*. J. Nanoparticle Res., 5(3-4): 323-332.

Zhao Y., Zhao D., Chen C., Wang X. 2013. *Enhanced photo-reduction and removal of Cr (VI) on reduced graphene oxide decorated with TiO_2 nanoparticles*. J Colloid Interface Sci, 405: 211-217.

Zulkali M.M.D., Ahmad A.L., Norulakmal N.H., Ovyza S.L. 2006. *Oryza sativa* L. *husk as heavy metal adsorbent: optimization with head as model solution*. J Biores Technol, 97(1): 21-25.